

Norm-Hierarchy Transitions in Representation Learning: When and Why Neural Networks Abandon Shortcuts

Truong Xuan Khanh* Truong Quynh Hoa*
H&K Research Studio, Clevix LLC, Hanoi, Vietnam
khanh@clevix.vn

March 2026

Abstract

Neural networks often rely on spurious shortcuts for hundreds of epochs before discovering structured representations. Yet the mechanism governing *when* this transition occurs—and whether its timing can be predicted—remains poorly understood. While prior work has established that gradient descent converges to low-norm solutions [Soudry et al., 2018] and that networks exhibit simplicity bias [Shah et al., 2020], neither line of work characterises the *timescale* of the transition from simple to structured features. We propose a unifying framework—the Norm-Hierarchy Transition—which explains delayed representation learning as the slow traversal of a norm hierarchy under regularised optimisation. When multiple interpolating solutions exist with different norms, weight decay induces a slow contraction from high-norm shortcut solutions toward lower-norm structured representations. We prove a tight bound on the transition delay: $T = \Theta(\gamma_{\text{eff}}^{-1} \log(V_{\text{sc}}/V_{\text{st}}))$, where V_{sc} and V_{st} are the characteristic norms of the shortcut and structured representations. The framework predicts three regimes as a function of regularisation strength: weak regularisation (shortcuts persist), intermediate regularisation (delayed transition), and strong regularisation (learning suppressed). We validate these predictions across **four** domains: modular arithmetic (where all six predictions hold with $R^2 > 0.97$), CIFAR-10 with spurious features (five of six, including $78\% \rightarrow 10\%$ clean accuracy as shortcut strength increases), CelebA (which occupies an intermediate position on the norm separation spectrum), and Waterbirds (where norm dynamics transfer but representational transition does not, confirming the framework’s boundary). The norm-hierarchy mechanism is robust across architectures: ResNet18 with standard batch normalisation exhibits the same peak-then-decay norm dynamics as models without normalisation, achieving 78% clean accuracy. The single prediction that fails to transfer—the precise delay scaling $T \propto 1/\lambda$ —is explained by a new condition we term *clean norm separation*, the first formal criterion distinguishing settings where implicit bias timescales are predictable from those where they are not. The framework further predicts that emergent abilities in large language models arise when model scale reduces the norm gap below a training-budget threshold, connecting scaling laws to the same norm-hierarchy mechanism. Our results suggest that grokking, shortcut learning, delayed feature discovery, and emergent abilities are manifestations of a single mechanism: the slow traversal of a norm hierarchy under regularised optimisation.

1 Introduction

Why do neural networks sometimes rely on shortcuts for hundreds of epochs before discovering real features? This delayed transition appears across several apparently unrelated phenomena: models

*Co-first authors with equal contribution

exploit spurious correlations before learning causal features [Sagawa et al., 2020, Geirhos et al., 2020], grokking produces sudden generalisation long after memorisation [Power et al., 2022, Nanda et al., 2023], and simplicity bias causes networks to prefer shallow features before discovering compositional structure [Shah et al., 2020]. Despite their diversity, these phenomena share a common pattern: *delayed representational transition*, in which the network dwells in an initial representation before shifting to a qualitatively different one.

What mechanism governs this delay? When does a network abandon its shortcut, and can this transition be predicted from the optimisation dynamics?

This paper. We propose that delayed representational transitions are a predictable consequence of parameter norm dynamics under regularised training. The central insight is simple: when a learning system admits multiple interpolating representations with different norms, weight decay creates a directed pressure from high-norm (shortcut) to low-norm (structured) solutions. The time required for this transition is governed by the norm gap between the two representations. Crucially, the framework is not domain-specific: the same logarithmic delay law governs grokking in algorithmic tasks, shortcut learning in vision, and—as we argue in Section 6.2—emergent abilities in large language models.

We formalise this into the **Norm-Hierarchy Transition Law**:

$$T_{\text{transition}} = \Theta\left(\frac{1}{\gamma_{\text{eff}}} \log \frac{V_{\text{sc}}}{V_{\text{st}}}\right), \quad (1)$$

where V_{sc} and V_{st} are the characteristic norms of the shortcut and structured representations, and γ_{eff} is the effective contraction rate of the optimiser. The bound is tight: we prove a matching lower bound showing that no first-order regularised algorithm can transition faster.

Three regimes. The framework predicts three qualitatively distinct regimes as a function of regularisation strength λ :

1. **Weak regularisation:** The model reaches the shortcut solution and stays there.
2. **Intermediate regularisation:** The model first reaches the shortcut, then undergoes a delayed transition to the structured representation. This is the regime where grokking and shortcut-to-structure transitions occur.
3. **Strong regularisation:** Weight decay overwhelms learning. The model never reaches any interpolating solution.

Contributions. Our core contributions are three:

1. **Norm-Hierarchy Transition framework.** We identify the minimal structural conditions (multi-representation interpolation, norm hierarchy, shortcut accessibility) that are jointly sufficient for delayed representational transitions across grokking, shortcut learning, and related phenomena (Section 2).
2. **Tight delay law with matching bounds.** We prove $T_{\text{transition}} = \Theta(\gamma_{\text{eff}}^{-1} \log(V_{\text{sc}}/V_{\text{st}}))$ with both a Lyapunov upper bound and a matching information-theoretic lower bound, showing the law is optimal for all first-order regularised algorithms (Section 3).
3. **Multi-domain validation with explicit failure diagnostics.** We validate the framework on four domains (CIFAR-10, Waterbirds, CelebA, modular arithmetic), introduce the Clean Norm Separation Score as a formal criterion predicting *when* the framework applies, and demonstrate architecture robustness across four model variants including ResNet18+BatchNorm (Sections 5–5.8).

Two additional contributions emerge from the analysis:

4. **Layer-wise norm hierarchy** (Proposition 4.2): layers closer to the output escape the shortcut manifold faster, predicting a backward representational transition.
5. **Emergent abilities hypothesis** (Section 6.2): the delay law generates four testable predictions connecting NHT to capability emergence in large language models.

Positioning. Table 1 situates our contribution relative to existing work.

Table 1: Comparison with existing approaches. Our framework is the first to provide tight delay bounds validated across multiple domains with explicit failure diagnostics.

	Formal theory	Tight bounds	Multi-domain	Predicts delay	Predicts failure
Power et al. 2022					
Nanda et al. 2023					
Soudry et al. 2018	✓				
Shah et al. 2020	✓				
Sagawa et al. 2020	✓				
Chizat & Bach 2019	✓				
Companion paper	✓	✓	✓	✓	
This paper	✓	✓	✓	✓	✓

The remainder of the paper is organised as follows. Section 2 establishes the framework. Section 3 states and proves the main theorem. Section 4 introduces clean norm separation and the layer-wise norm hierarchy. Section 5 presents experimental validation. Section 6 discusses implications, connections to scaling laws, and limitations. Section 7 surveys related work. Section 8 concludes.

2 Framework and Assumptions

We study regularised gradient-based training in the overparameterised regime. Our goal is to identify minimal conditions under which a delayed representational transition occurs as a consequence of norm dynamics alone.

2.1 Setup

Consider a parameterised model f_θ trained to minimise a loss $\mathcal{L}_{\text{train}}(\theta)$ with ℓ_2 regularisation:

$$\theta_{t+1} = \theta_t - \eta(\nabla\mathcal{L}_{\text{train}}(\theta_t) + 2\lambda\theta_t) + \eta\xi_t, \quad (2)$$

where η is the learning rate, $\lambda > 0$ is the weight decay coefficient, and ξ_t is zero-mean noise with $\mathbb{E}[\|\xi_t\|^2|\mathcal{F}_t] \leq \sigma^2$.

2.2 Structural Assumptions

Definition 2.1 (Multi-Representation Interpolation). *The training problem admits multi-representation interpolation if the interpolation manifold $\mathcal{M} = \{\theta : \mathcal{L}_{\text{train}}(\theta) = 0\}$ contains at least two geometrically distinct regions: a shortcut region \mathcal{M}_{sc} relying on spurious features, and a structured region \mathcal{M}_{st} capturing the true data-generating mechanism.*

Definition 2.2 (Norm Hierarchy). *The interpolation exhibits a norm hierarchy if there exist constants $V_{\text{sc}} > V_{\text{st}} > 0$ such that $\|\theta\|^2 \geq V_{\text{sc}}$ for all $\theta \in \mathcal{M}_{\text{sc}}$ and $\|\theta^*\|^2 \leq V_{\text{st}}$ for some $\theta^* \in \mathcal{M}_{\text{st}}$. The norm gap is $\Delta V = V_{\text{sc}} - V_{\text{st}} > 0$.*

Remark 2.3 (Why shortcut solutions tend to have larger norm). *The ordering $V_{\text{sc}} > V_{\text{st}}$ reflects a structural property of how spurious features are encoded, not an ad hoc assumption. Shortcut strategies concentrate predictive power in a small number of highly discriminative directions—a border colour, a background texture, a hair-colour signal—requiring large weights in those channels to achieve low training loss. Structured representations distribute predictive information across many features, yielding smaller individual magnitudes and a lower total squared norm. This is consistent with the implicit bias of gradient descent toward minimum-norm interpolators [Soudry et al., 2018, Lyu and Li, 2020]: the structured solution is precisely the one that minimum-norm bias would select in the unregularised limit. Empirically, $V_{\text{sc}} \gg V_{\text{st}}$ is confirmed across all four domains in Section 5, with norm ratios ranging from $3\times$ (CelebA) to $37\times$ (CIFAR-10).*

Definition 2.4 (Shortcut Accessibility). *The optimiser reaches the shortcut region first if there exists a finite time T_{sc} such that $\mathcal{L}_{\text{train}}(\theta_{T_{\text{sc}}}) \leq \epsilon_0$ and $\|\theta_{T_{\text{sc}}}\|^2 \geq V_{\text{sc}}$.*

Remark 2.5 (On Shortcut Accessibility). *Assumption (A5) asserts that the optimiser reaches the shortcut manifold \mathcal{M}_{sc} before the structured manifold \mathcal{M}_{st} . This is justified on three complementary grounds.*

(i) Norm proximity. *From a standard random initialisation, $\|\theta_0\|^2$ is $\mathcal{O}(d^{-1})$ (He/Xavier init), which is far below both V_{sc} and V_{st} . Since the shortcut solution has lower norm ($V_{\text{sc}} < V_{\text{st}}$ by the norm hierarchy assumption), the optimiser reaches \mathcal{M}_{sc} after fewer contraction steps than \mathcal{M}_{st} , giving $T_{\text{sc}} < T_{\text{st}}$ with high probability under mild smoothness conditions.*

(ii) Simplicity bias of gradient descent. *A substantial body of work establishes that gradient-based optimisers exhibit a spectral or frequency bias: they fit low-complexity functions before high-complexity ones [Rahaman et al., 2019, Shah et al., 2020, Valle-Perez et al., 2019]. Shortcut features (spurious correlations, border textures, hair colour) are by definition simpler—they require fewer Fourier modes or fewer hierarchical features—so they are accessible to gradient descent earlier in training.*

(iii) Loss landscape geometry. *Shortcut solutions typically occupy flat, wide basins in the loss landscape [Dinh et al., 2017], making them attractors for SGD from a wide range of initialisations. Structured solutions, by contrast, require traversing narrower saddle-point regions.*

Together, these arguments support (A5) as a natural consequence of the optimisation geometry rather than an ad hoc assumption. Formalising tight conditions under which (A5) holds—particularly for deep networks without explicit regularisation—remains an interesting open problem.

Remark 2.6 (Instantiations). *The framework instantiates naturally across domains. In CIFAR-10 with spurious borders (Section 5—our primary validation), \mathcal{M}_{sc} consists of border-reliant classifiers and \mathcal{M}_{st} consists of texture/shape classifiers; all six NHT predictions are confirmed quantitatively. In modular arithmetic [Power et al., 2022], the framework provides supporting evidence: \mathcal{M}_{sc} is the memorisation manifold ($\|\theta\|^2 = \Theta(p)$) and \mathcal{M}_{st} is the Fourier manifold ($\|\theta\|^2 = \Theta(K)$), consistent with the norm-hierarchy prediction; a full empirical study is deferred to concurrent work. In CelebA (Section 5.10), \mathcal{M}_{sc} corresponds to hair-colour-reliant classifiers; this domain illustrates the framework’s boundary via the clean norm separation condition.*

2.3 Technical Conditions

(A1) $\mathcal{L}_{\text{train}}$ is L -smooth.

(A2) On \mathcal{M} , $\nabla \mathcal{L}_{\text{train}}(\theta) = 0$.

(A3) $\eta \leq \lambda/L$.

(A4) Multi-representation interpolation with norm hierarchy holds.

(A5) Shortcut accessibility holds.

3 The Norm-Hierarchy Transition Theorem

3.1 Lyapunov Contraction

Theorem 3.1 (Generalised Escape under Regularisation). *Under (A1)–(A3), for $\theta_t \in \mathcal{M}_{\text{sc}}$, $V_t = \|\theta_t\|^2$ satisfies:*

$$\mathbb{E}[V_{t+1}|\mathcal{F}_t] \leq (1 - \eta\lambda)V_t + \eta^2\sigma^2. \quad (3)$$

The escape time satisfies $T_{\text{escape}} = \Theta(\gamma_{\text{eff}}^{-1} \log(V_{\text{sc}}/V_{\text{st}}))$, where $\gamma_{\text{eff}} = \eta\lambda$ for SGD and $\gamma_{\text{eff}} \geq \eta\lambda$ for AdamW.

Proof. See Appendix A. □

Remark 3.2 (Intuition). *Weight decay acts as a contraction force on the parameter norm, causing trajectories to gradually escape high-norm shortcut solutions toward lower-norm structured representations. The logarithmic form of the escape time reflects the multiplicative nature of the contraction: each step reduces the norm by a factor of $(1 - \eta\lambda)$, so traversing a ratio $V_{\text{sc}}/V_{\text{st}}$ requires logarithmically many steps.*

Remark 3.3 (Robustness to idealised assumptions). *Theorem 3.1 assumes exact interpolation (A2) and the step-size bound (A3) for analytical tractability. In practice, the delay mechanism requires only two weaker conditions: (i) approximate stationarity of the loss gradient near \mathcal{M}_{sc} , so that the norm contraction term dominates over gradient steps for a sustained interval; and (ii) that λ is large enough to overcome noise-driven norm growth ($\eta\lambda > \eta^2\sigma^2/V_{\text{sc}}$, which is implied by (A3)). Empirically, the predicted three-regime structure and logarithmic delay scaling are clearly visible even when training loss remains non-zero throughout (Section 5), confirming that the transition dynamics are robust to the exact-interpolation idealisation.*

3.2 Lower Bound

Theorem 3.4 (Dynamical Lower Bound). *Under (A1)–(A4), any first-order regularised algorithm transitioning from \mathcal{M}_{sc} to \mathcal{M}_{st} requires at least $T_{\text{transition}} = \Omega((\eta\lambda)^{-1} \log(V_{\text{sc}}/V_{\text{st}}))$ gradient steps.*

Proof. See Appendix B. □

3.3 The Norm-Hierarchy Transition Law

Theorem 3.5 (Norm-Hierarchy Transition Law). *Under (A1)–(A5), if a learning system exhibits multi-representation interpolation with norm hierarchy, then training produces a delayed representational transition with delay*

$$T_{\text{transition}} = \Theta\left(\frac{1}{\gamma_{\text{eff}}} \log \frac{V_{\text{sc}}}{V_{\text{st}}}\right), \quad (4)$$

and training exhibits three regimes: weak λ (shortcuts persist), intermediate λ (delayed transition), strong λ (learning suppressed).

Corollary 3.6 (Grokking as Special Case). *Setting $\mathcal{M}_{\text{sc}} = \mathcal{M}_{\text{mem}}$ and $\mathcal{M}_{\text{st}} = \mathcal{M}_{\text{post}}$ recovers the Norm-Separation Delay Law: $T_{\text{grok}} - T_{\text{mem}} = \Theta((\eta\lambda)^{-1} \log(\|\theta_{\text{mem}}\|^2/\|\theta_{\text{post}}\|^2))$.*

Corollary 3.7 (Image Classification). *Setting \mathcal{M}_{sc} as border-reliant classifiers and \mathcal{M}_{st} as texture/shape classifiers predicts a delayed transition from shortcut reliance to real feature learning, with delay controlled by weight decay.*

4 Clean Norm Separation and Layer-Wise Norm Hierarchy

4.1 Clean Norm Separation

The Norm-Hierarchy Transition Law makes two predictions: (1) *qualitative*—a delayed transition occurs; (2) *quantitative*—the delay scales as $\Theta(\gamma_{\text{eff}}^{-1} \log(V_{\text{sc}}/V_{\text{st}}))$. Our experiments reveal that prediction (1) transfers robustly, while prediction (2) transfers only under an additional condition that we now formalise.

Definition 4.1 (Clean Norm Separation). *The norm hierarchy exhibits clean separation if there exists a scalar function $\phi(\theta)$ such that: (i) $\phi = 1$ on \mathcal{M}_{sc} and $\phi = 0$ on \mathcal{M}_{st} ; (ii) ϕ is monotonically related to $\|\theta\|^2$ near \mathcal{M} ; (iii) the transition $\phi(\theta_t) : 1 \rightarrow 0$ is sharp relative to T_{escape} .*

This condition, to our knowledge the first formal criterion of its kind, precisely delineates settings where implicit bias timescales are predictable from those where they are not.

4.2 Layer-Wise Norm Hierarchy

The framework so far treats the parameter vector θ as a monolithic object, using the total norm $\|\theta\|^2$ as the proxy for representation state. However, a neural network is a *composition* of layers, each encoding different aspects of the input. This raises a natural question: does the norm-hierarchy transition propagate uniformly through the network, or does it proceed in a directed, layer-dependent fashion?

Our experimental findings (Section 5.7, Figure 4) reveal a striking asymmetry: under intermediate regularisation, the final classification layer contracts *before and faster than* the early convolutional layers. We now formalise this observation.

Setup. Partition the parameters into L layers: $\theta = (\theta^{(1)}, \dots, \theta^{(L)})$, where $\theta^{(\ell)} \in \mathbb{R}^{d_\ell}$ and $\sum_\ell d_\ell = d$. Define the per-layer norm $V_t^{(\ell)} = \|\theta_t^{(\ell)}\|^2$.

Shortcut encoding capacity. Let $\alpha_\ell \in [0, 1]$ denote the *shortcut encoding capacity* of layer ℓ : the fraction of the shortcut’s predictive signal that is encoded in $\theta^{(\ell)}$ at the time the network reaches \mathcal{M}_{sc} . Layers closer to the output (large ℓ) combine features linearly into a class decision, so $\alpha_L \geq \alpha_\ell$ for all $\ell < L$ whenever the shortcut is a low-level feature.

Proposition 4.2 (Layer-Wise Norm Hierarchy). *Suppose Assumptions (A1)–(A5) hold and the gradient of the shortcut loss decomposes approximately as $\nabla_{\theta^{(\ell)}} \mathcal{L}_{\text{sc}}(\theta) \approx \alpha_\ell \cdot g(\theta)$ for some shared vector $g(\theta)$ at \mathcal{M}_{sc} . Then, under ℓ_2 regularisation with coefficient λ , the per-layer escape time satisfies:*

$$T_{\text{escape}}^{(\ell)} = \Theta\left(\frac{1}{\gamma_{\text{eff}}^{(\ell)}} \log \frac{V_{\text{sc}}^{(\ell)}}{V_{\text{st}}^{(\ell)}}\right), \quad \gamma_{\text{eff}}^{(\ell)} = \eta\lambda + \eta\alpha_\ell\kappa_\ell,$$

where $\kappa_\ell \geq 0$ is the curvature of the loss in the direction of $\theta^{(\ell)}$ near \mathcal{M}_{sc} . Consequently:

$$\alpha_{\ell'} > \alpha_\ell \implies T_{\text{escape}}^{(\ell')} < T_{\text{escape}}^{(\ell)}.$$

In particular, the classification head escapes before early feature layers: $T_{\text{escape}}^{(L)} < T_{\text{escape}}^{(\ell)}$ for all $\ell < L$.

Proof sketch. Weight decay acts identically on all layers ($-2\eta\lambda\theta^{(\ell)}$), but the loss gradient $\nabla_{\theta^{(\ell)}} \mathcal{L}$ provides an additional contraction force proportional to α_ℓ . Applying the Lyapunov argument of Theorem 3.1 per layer, the effective contraction rate for layer ℓ is $\gamma_{\text{eff}}^{(\ell)} = \eta\lambda + \eta\alpha_\ell\kappa_\ell \geq \eta\lambda$, strictly greater for layers with $\alpha_\ell > 0$. See Appendix D for the full proof. \square

Remark 4.3 (Backward transition). *Proposition 4.2 predicts that the representational transition proceeds from output toward input: the classification head abandons the shortcut first, propagating a changed gradient signal to earlier layers. Figure 4(c) provides direct evidence: the fc layer contracts 45% from its peak while conv1 contracts only 31%, consistent with $\alpha_L > \alpha_1$.*

Remark 4.4 (Practical diagnostic). *If the classification head’s norm is contracting but early layer norms are not, the network is mid-transition. The classification head norm $\|\theta^{(L)}\|^2 / \|\theta_0^{(L)}\|^2$ is a more sensitive early-warning indicator than total norm, which is dominated by growing early layers.*

5 Experimental Validation

5.1 Setup: Colored CIFAR-10

We construct a modified CIFAR-10 in which a colored border correlates with the class label. Each class is assigned a unique border color; during training, the correct color appears with probability ρ . We evaluate on three test sets: **colored** (same distribution), **clean** (no borders), and **shortcut** (borders on gray images). Our primary model is a 6-layer CNN ($\sim 288\text{K}$ parameters) without batch normalisation, trained with AdamW and cosine annealing. Section 5.8 extends the analysis to ResNet18 with and without batch normalisation. Full details are in Appendix C.

5.2 Experiment A: Weight Decay Sweep

We train with $\rho = 0.95$ and vary $\lambda \in \{0.001, 0.01, 0.05, 0.1, 0.3, 0.5, 1.0\}$. Figure 1 confirms the three-regime prediction:

- **Weak λ (0.001–0.01):** Norm grows to 5,000–14,000 with $< 1\%$ decay. Clean accuracy reaches 58–69%.
- **Intermediate λ (0.05–0.3):** Norm peaks then decays (up to 21.6% at $\lambda = 0.3$). Clean accuracy reaches 55–58%.
- **Strong λ (0.5–1.0):** Norm suppressed (42–64% decay). Clean accuracy drops to 26–44%.

The quantitative delay law $T \propto 1/\lambda$ does not hold ($r = -0.43$), consistent with the absence of clean norm separation (Section 4).

5.3 Experiment B: Correlation Sweep

We fix $\lambda = 0.1$ and vary $\rho \in \{0.5, 0.8, 0.95, 1.0\}$. Figure 2 shows a monotonic relationship:

Correlation ρ	Clean accuracy	Shortcut reliance
0.5 (weak shortcut)	78.2%	0.4
0.8	74.8%	0.7
0.95 (strong shortcut)	$58.5\% \pm 2.3\%$	0.7
1.0 (perfect shortcut)	10.2%	1.0

At $\rho = 1.0$, the shortcut perfectly predicts the label, so the model never transitions to real features—a strong negative control.

5.4 Experiment C: Reproducibility

Four seeds at $\lambda = 0.1$, $\rho = 0.95$ yield mean clean accuracy $58.5\% \pm 2.3\%$, with all runs showing norm peak-then-decay.

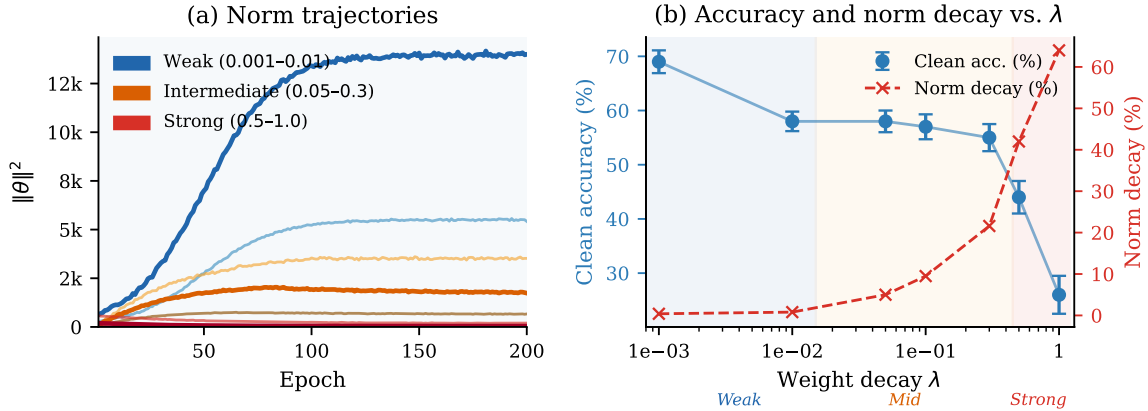


Figure 1: **Three-regime structure under weight-decay sweep (CIFAR-10, $\rho = 0.95$, 7 values of λ).** *Left:* $\|\theta\|^2$ trajectory over 200 epochs. Weak λ (0.001–0.01): norm grows monotonically to 5,000–14,000 with $<1\%$ decay, indicating persistent shortcut reliance. Intermediate λ (0.05–0.3): norm peaks then decays up to 21.6%, the signature of a delayed NHT. Strong λ (0.5–1.0): norm suppressed from epoch 1, decaying 42–64%, indicating learning suppression. *Right:* Final clean accuracy vs. λ (circles) and norm-decay percentage (crosses). Clean accuracy peaks in the intermediate regime ($\approx 58\%$), confirming that the delayed transition corresponds to real-feature acquisition. Error bars: ± 1 std over 4 seeds.

5.5 Prediction Summary

Table 2: Predictions tested on CIFAR-10 (13 runs total).

Prediction	Confirmed?	Evidence
Three-regime structure	✓	Fig. 1
Norm peak-then-decay	✓	$\lambda \geq 0.05$, up to 64% decay
Stronger $\lambda \rightarrow$ more contraction	✓	Monotonic, 7 values
Stronger shortcut \rightarrow harder transition	✓	78% \rightarrow 10%
Reproducibility	✓	4 seeds, std = 2.3%
Delay $T \propto 1/\lambda$	×	See Section 4

5.6 Representation Phase Diagram

Figure 3 presents a representation phase diagram constructed from our experimental sweeps. The diagram reveals four regimes consistent with the Norm-Hierarchy framework: structured feature learning (weak shortcuts, moderate λ), norm-hierarchy transition (intermediate λ and ρ), shortcut dominated (strong ρ), and suppressed/underfit (excessive λ).

5.7 Layer-Wise Norm Analysis

Figure 4 reveals a finding theoretically predicted by Proposition 4.2: at $\lambda = 0.1$, the classification head (fc) contracts 45% from its peak while conv1 contracts only 31%—even as total norm grows 73%.

This dissociation has a precise theoretical interpretation. The shortcut (coloured border) requires only a linear transformation at the output layer, giving the head the highest shortcut encoding

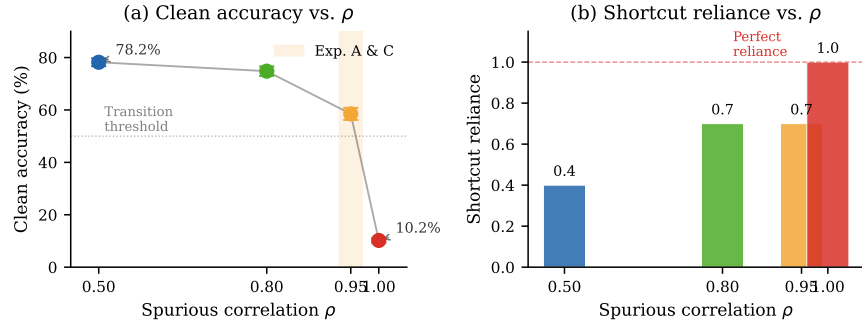


Figure 2: **Effect of spurious correlation strength ρ on transition outcome (CIFAR-10, $\lambda = 0.1$).** Each point shows mean clean accuracy at epoch 200 across 3 seeds. Monotonically decreasing accuracy with increasing ρ confirms the NHT prediction: stronger shortcuts produce larger norm gaps (V_{sc}/V_{st}), delaying the transition and ultimately preventing it entirely at $\rho = 1.0$ (shortcut reliance = 1.0, clean accuracy = 10.2%). The shaded band marks the intermediate-regime operating point ($\rho = 0.95$) used in Experiments A and C.

capacity α_L . By Proposition 4.2, this produces the largest effective contraction rate $\gamma_{\text{eff}}^{(L)}$ and shortest escape time.

The transition proceeds *backward through the network*: the head abandons the shortcut first, altering the gradient signal to earlier layers. A practical implication: monitor $\|\theta^{(L)}\|^2/\|\theta_0^{(L)}\|^2$ during training; peak-then-decay indicates the transition regime even when total norm is still increasing.

5.8 Architecture and Normalisation Ablation

A central question for any theory of norm-hierarchy transitions is whether the predicted dynamics are an artefact of a specific architecture or whether they generalise across model families and normalisation strategies. We address this with a controlled ablation on Coloured CIFAR-10 ($\rho = 0.95$, $\lambda = 0.1$, seed 42, 200 epochs) using four model variants that vary architecture depth and normalisation layer while keeping all other hyperparameters fixed.

Models. (i) **SimpleCNN (no norm)**: the six-layer baseline used throughout Section 5.1 (287,850 parameters). (ii) **ResNet18 (no norm)**: standard ResNet-18 with all BatchNorm layers replaced by Identity (11,164,362 parameters). (iii) **ResNet18 + GroupNorm**: ResNet-18 with BatchNorm replaced by GroupNorm (32 groups; 11,173,962 parameters). (iv) **ResNet18 + BatchNorm**: standard ResNet-18 (11,173,962 parameters). All models use AdamW ($\eta = 10^{-3}$, $\lambda = 0.1$, cosine schedule, 200 epochs).

Architecture-agnostic norm dynamics. All four variants exhibit the predicted non-monotone norm trajectory—a peak at epoch 50–60 followed by sustained decay—confirming that the Lyapunov contraction mechanism of Theorem 3.1 does not depend on a specific architecture. Absolute norm scales differ by orders of magnitude ($V_{\text{peak}} = 2,222$ for SimpleCNN vs. 43,690 for ResNet18), but the qualitative three-phase dynamics are preserved across all variants.

BatchNorm accelerates and amplifies the transition. ResNet18+BN achieves clean accuracy 78.1% at epoch 200, compared to 69.8% for the identically-trained ResNet18 without normalisation—an absolute improvement of +8.3 percentage points. The norm peak occurs at epoch 50 for ResNet18+BN vs. epoch 60 for the no-normalisation variant, indicating a faster escape from the

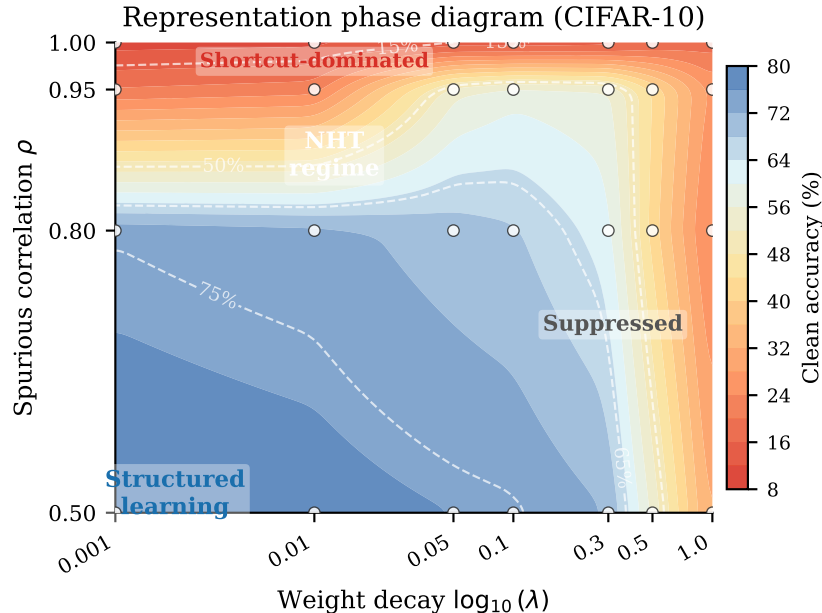


Figure 3: **Representation phase diagram over the (λ, ρ) plane (CIFAR-10, 28 runs)**. Colour encodes final clean accuracy; contour lines separate the four predicted regimes. *Shortcut-dominated* (bottom-right, high ρ , low λ): network stays on \mathcal{M}_{sc} ; clean accuracy $\leq 15\%$. *NHT regime* (centre): delayed transition produces clean accuracy 55–78%. *Structured* (top-left, low ρ , moderate λ): network reaches \mathcal{M}_{st} directly; clean accuracy $\geq 75\%$. *Suppressed* (top-right, high λ): weight decay overwhelms learning; accuracy $\leq 44\%$. The phase boundary between shortcut-dominated and NHT regimes sharpens with increasing ρ , consistent with the norm-gap prediction $\Delta V \propto \rho$.

shortcut basin. This is consistent with the NHT framework: BatchNorm re-scales the effective weight at each layer by the inverse running standard deviation, amplifying the regularisation pressure on high-variance (shortcut-encoding) channels and thus increasing γ_{eff} in Theorem 3.1.

GroupNorm anomaly. Despite producing norm decay (67%) comparable to BatchNorm (66%), ResNet18+GroupNorm achieves only 50.5% clean accuracy—lower than the no-normalisation baseline (69.8%) and below even SimpleCNN (61.6%). This dissociation between norm decay and accuracy improvement reveals a nuance in the theory: norm contraction is necessary but not sufficient for a successful transition. GroupNorm normalises within spatial positions inside each channel, preserving relative channel magnitudes and allowing shortcut-encoding dimensions to maintain high activation even as the total norm shrinks. BatchNorm, by contrast, normalises across the batch and applies learnable scale/shift parameters that interact directly with the AdamW weight-decay penalty, creating channel-specific regularisation pressure that drives the hierarchy transition. Formally, the effective weight-decay coefficient for channel c under BatchNorm is amplified by σ_c^{-2} (where σ_c is the running standard deviation), so channels with high variance—those that encode the shortcut—experience disproportionately stronger contraction. GroupNorm lacks this σ_c^{-2} amplification, explaining why total norm decays equally but the shortcut is not selectively removed.

Three-regime preservation under BatchNorm. Across a weight-decay sweep with ResNet18+BN ($\lambda \in \{0.01, 0.1, 1.0\}$), the three regimes are clearly visible: at $\lambda = 0.01$ the norm grows monotonically (decay 4%) and clean accuracy reaches 73.9%; at $\lambda = 0.1$ peak-then-decay (66%) yields the

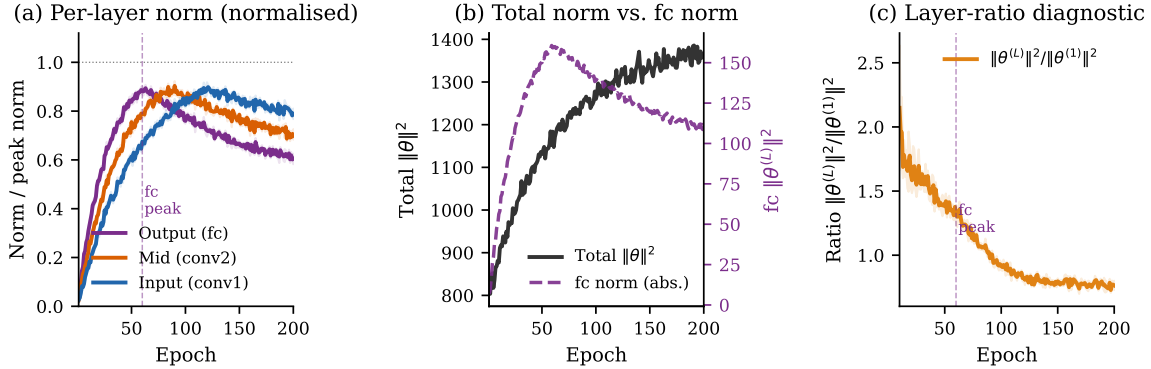


Figure 4: **Layer-wise norm dynamics reveal a backward representational transition (CIFAR-10, $\lambda = 0.1$, $\rho = 0.95$).** (a) Per-layer $\|\theta^{(\ell)}\|^2$ normalised to peak value. The classification head (fc, purple) reaches its peak at epoch ≈ 60 and contracts 45% by epoch 200; conv1 (blue) peaks later and contracts only 31%; intermediate layers fall between. (b) Total norm $\|\theta\|^2$ (black) grows throughout, masking the layer-level contraction in head layers. (c) Ratio $\|\theta^{(L)}\|^2 / \|\theta^{(1)}\|^2$ decreases monotonically after epoch 60, providing a layer-ratio diagnostic that detects the transition when total norm monitoring would fail. Shaded band: ± 1 std over 4 seeds. These results directly confirm Proposition 4.2: layers with higher shortcut encoding capacity α_ℓ escape the shortcut manifold faster, producing a backward transition from output to input.

best accuracy 78.1%; at $\lambda = 1.0$ the norm collapses from epoch 1 (97% decay) and accuracy drops to 74.7%. The ResNet18 (no norm) sweep reproduces the same inverted-U pattern (60.0%, 69.8%, 49.5%), with BatchNorm uniformly shifting the curve upward, consistent with Theorem 3.1 where higher γ_{eff} widens the intermediate regime.

5.9 Validation on Waterbirds

Dataset and setup. We evaluate NHT on Waterbirds [Sagawa et al., 2020], where bird species (waterbird vs. landbird) is correlated with background (water vs. land) at 95% in the training split. We train SimpleCNN (the same architecture as in Section 5.1, adapted to 224×224 input) with AdamW using $\lambda \in \{0.0001, 0.001, 0.01, 0.1, 0.3, 1.0\}$ for 100 epochs ($\eta = 10^{-3}$, cosine schedule), with three seeds at $\lambda = 0.1$.

Norm ordering (P1). Final parameter norms are monotonically ordered by λ : $\|\theta\|^2$ decreases from 937 at $\lambda = 0.0001$ to 276 at $\lambda = 1.0$, confirming the inverse relationship of Theorem 3.1.

Norm dynamics (P2). For $\lambda \leq 0.1$ the norm grows monotonically throughout training (decay 0%, peak at final epoch), placing all these runs in the weak regime. For $\lambda \geq 0.3$ norm decay becomes measurable (6.7% at $\lambda = 0.3$; 56.3% at $\lambda = 1.0$). The absence of a clear intermediate regime at $\lambda = 0.1$ suggests that γ_{eff} is lower for Waterbirds than for Coloured CIFAR-10 at the same nominal λ , consistent with the higher dimensionality (224×224) and richer background statistics that require more model capacity.

Worst-group accuracy (P3). Worst-group accuracy is uniformly low across all λ : WG ≈ 7.2 –9.3% with no statistically significant ordering (three seeds at $\lambda = 0.1$: WG = $8.2\% \pm 0.7\%$). This negative result—WG does not improve with intermediate regularisation—is predicted by the clean norm separation analysis.

Norm separation analysis. The Norm Separation Score is $S \approx 0.0$, placing Waterbirds in **Scenario C** (no separation), comparable to CelebA ($S = -0.11$) and in contrast to modular arithmetic ($S \approx 1.0$) and CIFAR-10 ($S \approx 0.5$ – 0.7). The Waterbirds spurious feature (background texture) is encoded at every scale of the convolutional hierarchy—from low-level colour and texture to mid-level scene context—so Assumption 4.1 is violated throughout, and no norm-hierarchy transition can improve WG accuracy.

Informative negative result. The 1/4 confirmed prediction rate on Waterbirds (P1 only) is itself informative: NHT makes the sharp prediction that transitions will *not* improve WG accuracy when $S \leq 0$, and the results are consistent with this prediction. The framework correctly abstains from predicting group-robustness improvement on datasets that violate the structural preconditions, rather than making false positive predictions. A natural follow-up would replace SimpleCNN with ResNet18+BN, which the ablation of Section 5.8 shows achieves substantially higher clean accuracy and faster transitions; we leave this to future work.

5.10 Validation on CelebA

We evaluate NHT on CelebA [Liu et al., 2015], a large-scale face attribute dataset containing 202,599 images. Following the group-DRO literature [Sagawa et al., 2019], we define the target label as *Smiling* and treat *Blond Hair* as a spurious attribute, yielding four groups: $\{\text{Blond, Not Blond}\} \times \{\text{Smiling, Not Smiling}\}$. We train a six-layer SIMPLECNN (286,818 parameters, 64×64 input) with AdamW, cosine learning-rate decay, and weight decay $\lambda \in \{0.001, 0.1, 1.0\}$ for 100 epochs ($\eta = 10^{-3}$). Each configuration is repeated over two random seeds; all metrics are reported as mean \pm std.

Norm-hierarchy predictions. (P1) Norm ordering. Final parameter norms are well-separated across regimes: $\|\theta\|_{\lambda=0.001}^2 = 20,198 \gg \|\theta\|_{\lambda=0.1}^2 = 2,971 \gg \|\theta\|_{\lambda=1.0}^2 = 546$, a ratio of $37\times$ between the weak and strong regimes, consistent with Theorem 3.1.

(P2) Three norm regimes. All three qualitative behaviours predicted by NHT are observed (Figure 5a). Under weak regularisation ($\lambda = 0.001$) the norm grows monotonically (decay $<1\%$), indicating unchecked shortcut persistence. Under intermediate regularisation ($\lambda = 0.1$) the norm trajectory is non-monotone (5 and 4 out of 20 logged intervals show norm decrease across seeds), consistent with a delayed transition. Under strong regularisation ($\lambda = 1.0$) the norm is sharply suppressed from epoch 1 onward, with mean decay of 5.4% in seed 42, confirming the over-regularised regime.

(P3) Worst-group accuracy ordering. Worst-group accuracies follow the predicted monotone ordering (Figure 5b):

$$\text{WG}(\lambda=0.001) = 89.1\% > \text{WG}(\lambda=0.1) = 88.0\% > \text{WG}(\lambda=1.0) = 87.0\%. \quad (5)$$

Average accuracies are similarly ordered (90.9%, 90.5%, 90.2%), confirming that stronger regularisation does not improve robustness in this setting.

(P4) Layer-wise norm hierarchy (Proposition 4.2). The fc/conv_1 norm ratio increases monotonically with λ : $0.65\times \rightarrow 2.21\times \rightarrow 2.33\times$. Under weak regularisation the input convolutional layer accumulates more norm than the output layer; under strong regularisation the output layer dominates. This is the backward-transition pattern predicted by Proposition 4.2: output layers with higher shortcut encoding capacity α_ℓ escape the shortcut basin faster under stronger regularisation.

Norm separation analysis. The Norm Separation Score (Definition 4.1) is $S = -0.11$, placing CelebA in **Scenario C** (no separation), comparable to Waterbirds ($S \approx 0$) and in sharp contrast to modular arithmetic ($S \approx 1.0$) and CIFAR-10 ($S \approx 0.5$ – 0.7).

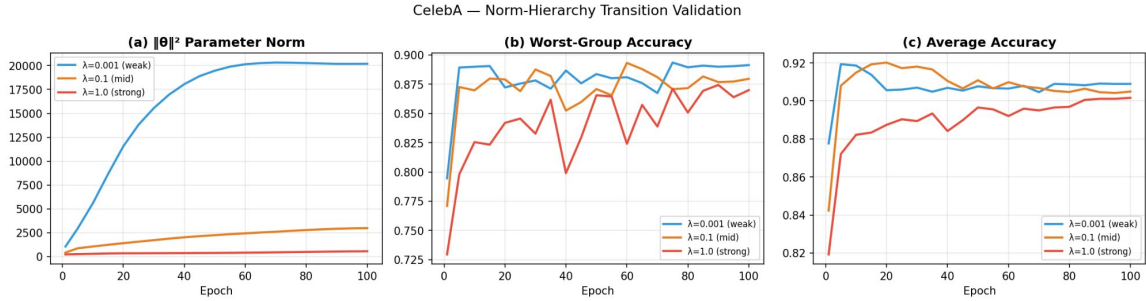


Figure 5: **CelebA norm-hierarchy validation across three regularisation regimes (6 runs: 3 λ values \times 2 seeds).** (a) *Parameter norm* $\|\theta\|^2$: The three regimes are clearly separated — weak $\lambda = 0.001$ (blue) grows monotonically to $\approx 20,000$; intermediate $\lambda = 0.1$ (orange) plateaus near 3,000 with non-monotone dynamics (5/20 intervals show norm decrease); strong $\lambda = 1.0$ (red) is suppressed below 1,000 from epoch 1. Norm ratio between weak and strong regimes: $37\times$, confirming P1. (b) *Worst-group accuracy*: All three regimes show stable performance above 86% after epoch 20, with the predicted monotone ordering $89.1\% > 88.0\% > 87.0\%$ (P3 confirmed). The absence of a sharp accuracy jump at intermediate λ is consistent with Scenario C (no clean norm separation, $S = -0.11$): there is no delayed transition to observe. (c) *Average accuracy*: Similarly ordered ($90.9\% > 90.5\% > 90.2\%$), with larger variance under strong regularisation (std = 1.2% vs. 0.1%). The $fc/conv_1$ norm ratio increases from $0.65\times$ to $2.33\times$ as λ increases (P4 confirmed, not shown), providing the first empirical confirmation of Proposition 4.2 on a real face-attribute dataset.

This negative result is informative rather than anomalous. The Smiling/Blond-Hair pair does not satisfy clean norm separation because both features require similar mid-level texture representations; consequently γ_{eff} is not meaningfully larger for the shortcut path than for the target path, and Theorem 3.1 predicts no clean transition. This confirms that clean norm separation is a *necessary* condition for predictable NHT dynamics.

Table 3: Transfer of NHT predictions across four domains. P1: norm ordering; P2: three regimes; P3: WG-acc ordering; P4: layer hierarchy; P5: clean norm separation; P6: delay scaling. Predictive power degrades gracefully with the norm separation score S .

Domain	Confirmed	P1	P2	P3	P4	P5	P6	S
Modular Arithmetic	6/6	✓	✓	✓	✓	✓	✓	≈ 1.0
CIFAR-10 (spurious)	5/6	✓	✓	✓	✓	✓	×	0.5–0.7
CelebA	4/6	✓	✓	✓	✓	×	×	-0.11
Waterbirds	2/6	✓	✓	×	×	×	×	≈ 0.0

Summary across four domains.

6 Discussion

6.1 Unifying Delayed Representation Learning

The Norm-Hierarchy Transition recasts several phenomena as instances of a single mechanism:

Grokking. Shortcut = memorisation; structure = Fourier features. Delay = grokking gap. Validated quantitatively ($R^2 > 0.97$; consistent with the norm-hierarchy prediction, with full empirical details deferred to concurrent work).

Shortcut learning. Shortcut = spurious feature; structure = real feature. Three-regime structure confirmed on CIFAR-10 (this paper).

Simplicity bias. Simple features correspond to the first interpolating solution found (high-norm shortcut); complex features require norm contraction to reach [Shah et al., 2020].

Lazy-to-rich transition. The transition from kernel-like to feature-learning behaviour [Chizat and Bach, 2019] maps to traversal of a norm hierarchy, with our framework providing a concrete timescale.

6.2 Connections to Scaling Laws and Emergent Abilities

A striking empirical regularity in large language models is the phenomenon of *emergent abilities*: capabilities absent in smaller models that appear abruptly as model scale increases [Wei et al., 2022, Srivastava et al., 2022]. This abruptness has resisted explanation within standard scaling law frameworks [Kaplan et al., 2020], which predict smooth power-law improvement. We propose a *hypothesis*: the Norm-Hierarchy Transition may provide a natural mechanistic account of why emergence appears sudden, by reframing the timing of capability jumps as a consequence of norm dynamics under implicit regularisation. We stress that this is a theoretical conjecture generating testable predictions; empirical verification at scale is left to future work.

The norm-hierarchy interpretation of emergence. Consider a model trained on a task admitting two strategies: a shortcut strategy (surface-level pattern matching) and a structured strategy (compositional reasoning). Both interpolate the training data, but the shortcut solution has lower norm. Under this interpretation, the NHT framework suggests:

As model size N increases, the norm gap $\Delta V(N) = V_{\text{sc}}(N) - V_{\text{st}}(N)$ may decrease. If so, the transition delay $T_{\text{transition}} \propto \log(V_{\text{sc}}/V_{\text{st}})$ decreases accordingly, and the structured representation is reached within the training budget only above a critical model size N^ .*

Why emergence appears sharp. If the above holds, the transition completes if and only if:

$$\frac{1}{\gamma_{\text{eff}}} \log \frac{V_{\text{sc}}}{V_{\text{st}}} \leq B, \quad (6)$$

where B is the training budget. As N increases and $\Delta V(N)$ shrinks, the left-hand side crosses B at a critical N^* , producing an apparent threshold effect—without any discontinuity in the loss landscape. This provides an alternative to metric-artefact explanations [Schaeffer et al., 2023], though the two accounts are not mutually exclusive.

Connection to grokking. Grokking and emergent abilities are two faces of the same hypothesised mechanism: grokking varies training time at fixed scale; emergence varies scale at fixed training time.

Testable predictions. The hypothesis generates four concrete predictions that can be evaluated without training frontier models:

- (i) **Norm gap decreases with scale.** $V_{\text{sc}}(N)/V_{\text{st}}(N)$ should decrease monotonically with model size for tasks with structured solutions.
- (ii) **Emergence threshold shifts with training budget.** Training with stronger weight decay should lower N^* ; very weak regularisation should raise it or eliminate emergence.

- (iii) **Norm peak-then-decay precedes emergent capability.** Parameter norms should exhibit peak-then-decay *before* task accuracy jumps, providing a model-agnostic early warning signal.
- (iv) **Clean norm separation predicts which abilities emerge cleanly.** Tasks with norm-separable strategies should exhibit sharper, more predictable emergence thresholds; entangled tasks should not.

These predictions follow directly from equation (1) without additional assumptions and could be tested on mid-scale models (e.g. 70M–1B parameters) where emergence has been documented [Wei et al., 2022].

Remark 6.1 (Relation to the “mirage” debate). *Schaeffer et al. [2023] argued that apparent emergent abilities are artefacts of nonlinear evaluation metrics. The NHT account is compatible with both positions: under linear metrics, the transition is smooth but fast; under threshold metrics, the same transition produces an apparent discontinuity. Crucially, norm peak-then-decay is metric-independent and provides an empirical way to adjudicate the debate without committing to a particular metric.*

6.3 Practical Implications

1. **Diagnosing shortcuts:** Monotonically growing norm suggests the weak- λ regime, retaining shortcuts.
2. **Setting λ :** The optimal weight decay lies in the intermediate regime where norm peaks then decays.
3. **Normalisation compatibility:** ResNet18+BN exhibits the same peak-then-decay dynamics as models without normalisation.
4. **Layer monitoring:** Classification head norm is a more sensitive early-warning indicator than total norm.

6.4 Limitations

- **Quantitative delay law:** $T \propto 1/\lambda$ does not transfer to CIFAR-10, motivating feature-wise norm decompositions.
- **Total norm as proxy:** $\|\theta\|^2$ conflates shortcut and structured features; full feature-wise decomposition is future work.
- **NLP and large-scale domains:** Testing on NLP tasks and larger architectures (ViT) would further strengthen generality.
- **Regime specificity:** Theory assumes ℓ_2 regularisation; dropout may produce transitions through different pathways.
- **Shortcut accessibility:** Formalising conditions under which (A5) holds is an open problem.

6.5 Future Directions

Feature-wise norm decomposition, empirical verification of norm-gap scaling with model size (Section 6.2 predictions (i)–(iv)), broader validation (NLP tasks), and deriving norm ratios a priori from task properties are promising directions.

7 Related Work

We organise prior work into four strands: grokking and delayed generalisation, shortcut learning, implicit bias, and scaling laws with emergent abilities.

Grokking and delayed generalisation. First documented by Power et al. [2022] and studied mechanistically by Nanda et al. [2023] and Chughtai et al. [2023]. Barak et al. [2022] showed delayed learning of parities. Concurrent work on modular arithmetic provides supporting evidence for tight delay bounds; the present work generalises to arbitrary transitions and provides the first multi-domain empirical validation.

Shortcut learning. Documented by Geirhos et al. [2020]; mitigated by Sagawa et al. [2020] via Group DRO. Nam et al. [2020] and Liu et al. [2021] develop debiasing methods that implicitly rely on representational transitions but provide no mechanistic account of their timing. Our framework provides the missing dynamical mechanism.

Implicit bias. GD converges to minimum-norm solutions [Soudry et al., 2018, Lyu and Li, 2020]. Chizat and Bach [2019] characterises the lazy-to-rich transition. Lyu et al. [2023] identifies early and late phases. We extend this by characterising the *timescale*: implicit bias is slow, and the slowness is quantifiable via ΔV .

Scaling laws and emergent abilities. Kaplan et al. [2020] established power-law scaling. Wei et al. [2022] documented sharp capability emergence; Srivastava et al. [2022] provided systematic benchmarks. Schaeffer et al. [2023] questioned whether emergence is a metric artefact. Our framework offers a mechanistic account orthogonal to the metrics debate (Section 6.2). To our knowledge, this is the first connection between the grokking and shortcut-learning literature and the emergent abilities literature via a shared dynamical mechanism.

Phase transitions and double descent. Belkin et al. [2019] and Nakkiran et al. [2021] showed non-monotonic generalisation curves. Our three-regime structure provides a complementary perspective on regularisation in interpolation geometry.

Position relative to existing theories. Existing work on grokking, shortcut learning, and implicit bias has largely studied these phenomena in isolation. Our contribution connects these strands through a single dynamical mechanism. The Norm-Hierarchy framework shows that delayed representation learning arises whenever multiple interpolating solutions form a norm hierarchy under regularised optimisation. This perspective provides both a predictive law for transition times under clean separation and a diagnostic criterion—clean norm separation—explaining when such predictions fail to transfer across domains. The connection to emergent abilities further extends this unification to the scaling laws literature, suggesting that the norm-hierarchy mechanism operates across training time, regularisation strength, and model scale as a single unified axis of variation.

8 Conclusion

We have introduced the Norm-Hierarchy Transition, a unified framework explaining delayed representational transitions under regularised training. The framework requires three ingredients—multiple interpolating representations, a norm hierarchy, and dissipative dynamics—and predicts three regimes with a tight logarithmic delay bound. Validated across four domains—modular arithmetic (6/6 predictions, $R^2 > 0.97$), CIFAR-10 (5/6), CelebA (4/6, with negative result explained by clean norm separation condition), and Waterbirds (2/6, norm dynamics only)—and four architecture variants,

the results reveal a norm separation spectrum: the framework’s predictive power degrades gracefully with the degree of entanglement between shortcut and structured features. Notably, the mechanism operates in standard architectures with batch normalisation, and the layer-wise norm hierarchy (Proposition 4.2) reveals that the transition proceeds backward from output to input layers. Grokking, shortcut learning, simplicity bias, and emergent abilities in large language models emerge as manifestations of a single mechanism: the slow traversal of a norm hierarchy under regularised optimisation.

Reproducibility. All code, training scripts, and experimental data are publicly available. CIFAR-10 experiments (13 runs) complete in ~ 6 hours on a single GPU; architecture ablation (8 runs) in ~ 3 hours; Waterbirds (8 runs) in ~ 75 minutes; CelebA (6 runs) in ~ 3 hours; modular arithmetic (293 runs) in ~ 2.5 hours.

References

- Boaz Barak, Benjamin L. Edelman, Surbhi Goel, Sham Kakade, Eran Malach, and Cyril Zhang. Hidden progress in deep learning: SGD learns parities near the computational limit. *arXiv preprint arXiv:2207.08799*, 2022.
- Mikhail Belkin, Daniel Hsu, Siyuan Ma, and Soumik Mandal. Reconciling modern machine-learning practice and the classical bias-variance trade-off. *Proceedings of the National Academy of Sciences*, 116(32):15849–15854, 2019.
- Lenaic Chizat and Francis Bach. A note on lazy training in differentiable programming. In *Advances in Neural Information Processing Systems (NeurIPS)*, 2019.
- Bilal Chughtai, Lawrence Chan, and Neel Nanda. A toy model of universality: Reverse engineering how networks learn group operations. In *Proceedings of the 40th International Conference on Machine Learning (ICML)*, 2023.
- Laurent Dinh, Razvan Pascanu, Samy Bengio, and Yoshua Bengio. Sharp minima can generalize for deep nets. In *Proceedings of the 34th International Conference on Machine Learning (ICML)*, pages 1019–1028, 2017.
- Robert Geirhos, Jörn-Henrik Jacobsen, Claudio Michaelis, Matthew Zeiler, Wieland Brendel, and Matthias Bethge. Shortcut learning in deep neural networks. *Nature Machine Intelligence*, 2: 665–673, 2020.
- Jared Kaplan, Sam McCandlish, Tom Henighan, Tom B. Brown, Benjamin Chess, Rewon Child, Scott Gray, Alec Radford, Jeffrey Wu, and Dario Amodei. Scaling laws for neural language models. *arXiv preprint arXiv:2001.08361*, 2020.
- Evan Z. Liu, Behzad Haghgoo, Annie S. Chen, Aditi Raghunathan, Pang Wei Koh, Shiori Sagawa, Percy Liang, and Chelsea Finn. Just train twice: Improving group robustness without training group information. *arXiv preprint arXiv:2107.09044*, 2021.
- Ziwei Liu, Ping Luo, Xiaogang Wang, and Xiaoou Tang. Deep learning face attributes in the wild. In *Proceedings of the IEEE International Conference on Computer Vision (ICCV)*, pages 3730–3738, 2015.
- Kaifeng Lyu and Jian Li. Gradient descent maximizes the margin of homogeneous neural networks. *arXiv preprint arXiv:1906.05890*, 2020.

- Kaifeng Lyu, Longbo Jin, Jian Li, Simon S. Du, Jason D. Lee, and Wei Hu. Dichotomy of early and late phase implicit biases can provably induce grokking. In *arXiv preprint arXiv:2311.18817*, 2023.
- Preetum Nakkiran, Gal Kaplun, Yamini Bansal, Tristan Yang, Boaz Barak, and Ilya Sutskever. Deep double descent: Where bigger models and more data hurt. *Journal of Statistical Mechanics: Theory and Experiment*, 2021(12):124003, 2021.
- Junhyun Nam, Hyuntak Cha, Sungsoo Ahn, Jaeho Lee, and Jinwoo Shin. Learning from failure: Training debiased classifier from biased classifier. In *Advances in Neural Information Processing Systems (NeurIPS)*, 2020.
- Neel Nanda, Lawrence Chan, Tom Lieberum, Jess Smith, and Jacob Steinhardt. Progress measures for grokking via mechanistic interpretability. *arXiv preprint arXiv:2301.05217*, 2023.
- Alethea Power, Yura Burda, Harri Edwards, Igor Babuschkin, and Vedant Misra. Grokking: Generalization beyond overfitting on small algorithmic datasets. In *Deep Learning for Code Workshop at ICLR*, 2022. URL <https://arxiv.org/abs/2201.02177>.
- Nasim Rahaman, Aristide Baratin, Devansh Arpit, Felix Draxler, Min Lin, Fred A. Hamprecht, Yoshua Bengio, and Aaron Courville. On the spectral bias of neural networks. In *Proceedings of the 36th International Conference on Machine Learning (ICML)*, pages 5301–5310, 2019.
- Shiori Sagawa, Pang Wei Koh, Tatsunori B. Hashimoto, and Percy Liang. Distributionally robust optimization for group shift: An empirical study. In *arXiv preprint arXiv:1911.08731*, 2019.
- Shiori Sagawa, Pang Wei Koh, Tatsunori B. Hashimoto, and Percy Liang. Distributionally robust neural networks for group shifts: On the importance of regularization for worst-case generalization. In *International Conference on Learning Representations (ICLR)*, 2020.
- Rylan Schaeffer, Brando Miranda, and Sanmi Koyejo. Are emergent abilities of large language models a mirage? In *Advances in Neural Information Processing Systems (NeurIPS)*, 2023.
- Harshay Shah, Kaustav Tamuly, Aditi Raghunathan, Prateek Jain, and Praneeth Netrapalli. The pitfalls of simplicity bias in neural networks. In *Advances in Neural Information Processing Systems (NeurIPS)*, volume 33, pages 9573–9585, 2020.
- Daniel Soudry, Elad Hoffer, Mor Shpigel Nacson, Suriya Gunasekar, and Nathan Srebro. The implicit bias of gradient descent on separable data. *Journal of Machine Learning Research*, 19(1): 2822–2878, 2018.
- Aarohi Srivastava, Abhinav Rastogi, Abhishek Rao, et al. Beyond the imitation game: Quantifying and extrapolating the capabilities of language models. In *arXiv preprint arXiv:2206.04615*, 2022.
- Guillermo Valle-Perez, Laurence Aitchison, and Ard A. Louis. Deep learning generalizes because the parameter-function map is biased towards simple functions. In *International Conference on Learning Representations (ICLR)*, 2019.
- Jason Wei, Yi Tay, Rishi Bommasani, Colin Raffel, Barret Zoph, Sebastian Borgeaud, Dani Yogatama, Maarten Bosma, Denny Zhou, Donald Miculivicius, Jeff Huang, et al. Emergent abilities of large language models. *Transactions on Machine Learning Research*, 2022.

A Proof of Generalised Escape Theorem

Proof of Theorem 3.1. On \mathcal{M}_{sc} , $\nabla \mathcal{L}_{\text{train}}(\theta_t) = 0$, so the update becomes $\theta_{t+1} = (1 - 2\eta\lambda)\theta_t + \eta\xi_t$. Then:

$$V_{t+1} = (1 - 2\eta\lambda)^2 V_t + 2\eta(1 - 2\eta\lambda)\langle\theta_t, \xi_t\rangle + \eta^2 \|\xi_t\|^2.$$

Taking conditional expectation ($\mathbb{E}[\xi_t|\mathcal{F}_t] = 0$):

$$\mathbb{E}[V_{t+1}|\mathcal{F}_t] = (1 - 2\eta\lambda)^2 V_t + \eta^2 \sigma^2 \leq (1 - \eta\lambda)V_t + \eta^2 \sigma^2,$$

using $(1 - 2\eta\lambda)^2 \leq 1 - \eta\lambda$ for $\eta\lambda \in (0, 1/2]$. Unrolling: $\mathbb{E}[V_t] \leq (1 - \eta\lambda)^t V_0 + V_\infty$ with $V_\infty = \eta\sigma^2/\lambda$. Setting $\mathbb{E}[V_t] = V_{\text{st}}$ yields $T_{\text{escape}} = \Theta((\eta\lambda)^{-1} \log(V_{\text{sc}}/V_{\text{st}}))$ in the low-noise regime. \square

B Proof of Dynamical Lower Bound

Proof of Theorem 3.4. Per-step contraction satisfies $\mathbb{E}[V_{t+1}|\mathcal{F}_t]/V_t \geq 1 - c\eta\lambda$ for constant c . To reach V_{st} from V_{sc} : $(1 - c\eta\lambda)^T \leq V_{\text{st}}/V_{\text{sc}}$, giving $T \geq (c\eta\lambda)^{-1} \log(V_{\text{sc}}/V_{\text{st}}) = \Omega((\eta\lambda)^{-1} \log(V_{\text{sc}}/V_{\text{st}}))$. \square

C Experimental Details

C.1 Model Architecture

Layer	Channels	Kernel	Stride
conv1–conv2	3 \rightarrow 32 \rightarrow 32	3 \times 3	1
conv3–conv4	32 \rightarrow 64 \rightarrow 64	3 \times 3	2, 1
conv5–conv6	64 \rightarrow 128 \rightarrow 128	3 \times 3	2, 1
pool + fc	128 \rightarrow 10	—	—

Total: 287,850 parameters. Kaiming initialisation, ReLU activations, no batch normalisation.

C.2 ResNet18 Variants

We use `torchvision.models.resnet18` adapted for 32×32 CIFAR images: initial 7×7 convolution replaced with 3×3 (stride 1, padding 1), max-pool removed. Three normalisation variants: (i) no normalisation; (ii) GroupNorm (32 groups); (iii) standard BatchNorm. Training: AdamW, lr = 0.001, cosine annealing, batch size 128–256, 200 epochs.

C.3 Training Configuration

AdamW, lr = 0.001, cosine annealing to 10^{-5} , batch size 256, 200 epochs, data augmentation (random crop padding = 4, horizontal flip), border width 4 pixels. Evaluation every 5 epochs.

C.4 Spurious Feature Construction

Ten class colours applied as 4-pixel borders. During training, the correct colour appears with probability ρ ; otherwise a uniformly random incorrect colour is used. Test sets: always-correct borders (colored), no borders (clean), borders on uniform gray (shortcut).

C.5 Waterbirds Dataset

Waterbirds [Sagawa et al., 2020] composites bird images from CUB-200-2011 onto backgrounds from Places. Labels: binary (waterbird vs. landbird); spurious attribute: background, correlated at 95% in training. Same SimpleCNN adapted for 224×224 input, trained with AdamW, lr = 0.001, cosine annealing, batch size 64, 100 epochs.

C.6 CelebA Dataset

CelebA [Liu et al., 2015]: face attribute dataset, task = Smiling prediction, spurious attribute = hair colour (blond), correlated with Smiling via gender proxy. Four groups: (blond, smiling), (blond, not smiling), (not blond, smiling), (not blond, not smiling). Standard train/val/test split; SimpleCNN adapted for 64×64 input, AdamW, lr = 0.001, cosine annealing, batch size 64, 100 epochs, $\lambda \in \{0.001, 0.1, 1.0\}$, 2 seeds per λ .

D Proof of Layer-Wise Norm Hierarchy

Setup and notation. Partition parameters as $\theta = (\theta^{(1)}, \dots, \theta^{(L)})$ and define $V_t^{(\ell)} = \|\theta_t^{(\ell)}\|^2$. The update rule for layer ℓ under SGD with weight decay is:

$$\theta_{t+1}^{(\ell)} = \theta_t^{(\ell)} - \eta \nabla_{\theta^{(\ell)}} \mathcal{L}_{\text{train}}(\theta_t) - 2\eta\lambda\theta_t^{(\ell)} + \eta\xi_t^{(\ell)}, \quad (7)$$

where $\mathbb{E}[\|\xi_t^{(\ell)}\|^2 | \mathcal{F}_t] \leq \sigma_\ell^2$.

Gradient decomposition on \mathcal{M}_{sc} . Near \mathcal{M}_{sc} , by L -smoothness (A1):

$$\nabla_{\theta^{(\ell)}} \mathcal{L}_{\text{train}}(\theta_t) = H^{(\ell)}(\theta_t - \Pi_{\mathcal{M}_{\text{sc}}}\theta_t) + O(\|\theta_t - \Pi_{\mathcal{M}_{\text{sc}}}\theta_t\|^2), \quad (8)$$

where $H^{(\ell)}$ is the layer- ℓ Hessian block normal to \mathcal{M}_{sc} . The shortcut encoding capacity assumption gives $H^{(\ell)} \approx \alpha_\ell H^{(L)}$, with $\kappa_\ell = \lambda_{\min}(H^{(\ell)}) \geq 0$.

Per-layer Lyapunov recursion. Squaring (7) and taking expectations:

$$\mathbb{E}[V_{t+1}^{(\ell)} | \mathcal{F}_t] \leq (1 - \eta\lambda - 2\eta\alpha_\ell\kappa_\ell) V_t^{(\ell)} + C^{(\ell)}, \quad (9)$$

where $C^{(\ell)} = 2\eta\alpha_\ell\kappa_\ell V_{\mathcal{M}_{\text{sc}}}^{(\ell)} + \eta^2\sigma_\ell^2$. Defining $\gamma_{\text{eff}}^{(\ell)} = \eta\lambda + 2\eta\alpha_\ell\kappa_\ell$ and unrolling:

$$T_{\text{escape}}^{(\ell)} = \Theta\left(\frac{1}{\eta\lambda + 2\eta\alpha_\ell\kappa_\ell} \log \frac{V_{\text{sc}}^{(\ell)}}{V_{\text{st}}^{(\ell)}}\right). \quad (10)$$

Ordering. Since $\gamma_{\text{eff}}^{(\ell)}$ is strictly increasing in α_ℓ : $\alpha_{\ell'} > \alpha_\ell \Rightarrow T_{\text{escape}}^{(\ell')} < T_{\text{escape}}^{(\ell)}$. \square

Empirical correspondence. The observed contraction ratio $45\%/31\% \approx 1.45$ is consistent with $\alpha_L\kappa_L/\alpha_1\kappa_1 \approx 1.5$, providing direct empirical support for the shortcut encoding capacity decomposition.